Progress In Electromagnetics Research M, Vol. 51, 139–146, 2016

Efficient Localization Algorithm of Mixed Far-Field and Near-Field Sources Using Uniform Circular Array

Bing Xue[1, 2, *], Guangyou Fang[1, 2], and Yicai Ji[1, 2]

Abstract—An efficient algorithm based on high-order cumulant is addressed for the scenarios where both far-field and near-field narrow-band signals may exist synchronously. The first matrix built by four-order cumulant is utilized to estimate the two dimensional direction-of-arrivals (DOAs) using the orthogonal projection matrix of the signal subspace and the virtual steering matrix. Then, the second matrix built by four-order cumulant is decomposed to get the noise subspace using the eigen decomposition. Meanwhile, a virtual steering matrix is used to distinguish far-field signals (FFSs) from near-field signals (NFSs). And one-dimensional MUSIC algorithm is used to estimate the range of the NFSs. Compared to the TSMUSIC, the proposed algorithm can provide high resolution for the DOAs. In addition, there is higher accuracy for the DOA of NFS in the proposed algorithm than that in TSMUSIC and in TSMD. Simulation results are carried out to certify the performance of the proposed algorithm.

1. INTRODUCTION

There has been considerable interest in the passive sources localization with an array of spatially separated sensors, which has many important application areas such as radar, guidance systems and sonar [1]. Various high performance algorithms such as MUSIC [2] and ESPRIT [3] have been used to deal with the DOA estimation of the FFSs. However, the both DOA and range of the source that is localized at the Fresnel region of the array aperture need be considered in some practical applications like lightening localization and speaker guidance systems [4], each source may be in the near field or the far field of the sensor position. Hence, when the classical algorithms may fail in such scenarios, several solutions are available to process the mixed sources localization. Using two high dimensional cumulant matrices of the sensor outputs, Liang and Liu [4] provided a two-stage MUSIC algorithm to solve the mix sources localization problem of the high resolution, which has high computational complexity and cannot classify the FFSs and NFSs in similar DOA. Wang et al. [5] used the mixed-order MUSIC algorithm to decline the computational complexity and improved the accuracy. Jiang et al. [6] gave an algorithm that estimates DOAs of all FFSs and NFSs by ESPRIT, distinguishes the FFSs and NFSs and estimates the range of NFSs by MUSIC. Liu and Sun [7] used the spatial differencing technique to classify the NFSs from the mixed sources after the estimations of FFSs, which has the higher accuracy, classify the mixed signals successfully and lower computational load. The algorithm in [8] built the optimization problem to get the estimation function used to obtain the DOA and estimated the range of the source by the minimum variance distortionless response (MVDR). Yet, the aforementioned high resolution algorithms are all aimed at two dimensional localization (elevation DOA and range). For some three dimensional problems (azimuth angle, elevation angle and range), they may fail in mixed sources localization so that we need to have an increase for the performances.

Received 24 August 2016, Accepted 14 October 2016, Scheduled 30 October 2016
* Corresponding author: Bing Xue (xuebing14@mails.ucas.ac.cn).
[1] Institute of Electronics, Chinese Academy of Sciences, Beijing 100190, China. [2] Key Laboratory of Electromagnetic Radiation and Sensing Technology, Chinese Academy of Sciences, Beijing 100190, China.

Recently, there is a significant amount of attention paid to the three dimensional localization (two dimensional DOA). Two parallel uniform linear arrays (ULAs) were used in [9] to estimate the two-dimensional direction (azimuth angle, elevation angle) for noncoherent and coherent signals by the orthogonal projector. An L-shaped ULA was used in [10] to estimate the two dimensional DOAs for noncoherent signals using a computational efficient subspace-based algorithm. Wu et al. [11] presented multiple near-field sources localization using the two-stage MUSIC (TSMUSIC) by UCA. And Jung and Lee [12] gave an easy way to calculate the three-dimensional information of a single source. UCA is preferable over uniform linear array because of its 360° azimuthal coverage, additional angle information and unchanged directional pattern [11] for estimating mixed sources. So, in this paper, we choose the UCA to estimate the mixed source locations. The novel solution includes three stages: 1) UCA is used to estimate the mixed sources three dimensional localization. We give the mathematical model for this situation, which is similar to the model in [11–13]. 2) Two useful four-order cumulant matrices for UCA are built to distinguish the NFSs and FFSs, which can realize a more reasonable classification of the signals types than correlation function. 3) The virtual steering matrices are built to estimate the DOAs and the ranges, respectively. And the orthogonal projector is used in MUSIC, which can provide the great estimation accuracy and low computing complexity.

2. MIXED FAR-FIELD AND NEAR-FIELD SIGNAL MODEL

We consider the narrow-band signals (N_F far-field signals and N_N near-field signals) impinging on a UCA [11] with radius R and M identical omnidirectional sensors, and the array center is the phase reference point. Without loss of the propagation, all the sensors are employed on the xy-plane, while the FFSs are located at (θ_i, φ_i) and the NFSs located at $(\theta_i, \varphi_i, r_i)$, where $\theta_i \in [0, 2\pi)$ are the azimuth angles measured counterclockwise from the x axis; $\varphi_i \in [0, \pi/2)$ are the elevation angles measured downward from the z axis; r_i is the range measured from the UCA centre and $i = 1, 2, \ldots, N$. The received signal of the UCA by the k-th sensor can be expressed as

$$x_k(t) = \sum_{i=1}^{N_N} s_i(t) e^{\frac{j2\pi}{\lambda}\{r_i - r_k(\theta_i,\varphi_i,r_i)\}} + \sum_{i=1+N_N}^{N_N+N_F} s_i(t) e^{\frac{j2\pi R}{\lambda}\psi_{k,i}(\theta_i,\varphi_i)} + n(t) \tag{1}$$

where $k = 1, 2, \ldots, M$, $s_i(t)$ is the i-th source signal, $n(t)$ the additive sensor noise, and $\psi_{k,i}(\theta_i, \varphi_i) = \cos(\gamma_k - \theta_i)\sin(\varphi_i)$ with $\gamma_k = 2\pi k/M$ being the angle of the k-th sensor measured counterclockwise from the x-axis. λ is the wavelength of the source and $r_k(\theta_i, \varphi_i, r_i)$ the distance between the i-th source and the k-th sensor, which can be written as

$$r_k(\theta_i, \varphi_i, r_i) = \sqrt{r_i^2 - R^2 - 2r_i R\psi_{k,i}(\theta_i, \varphi_i)} \tag{2}$$

According to the Taylor series expansion, Eq. (2) can be approximated as

$$r_k(\theta_i, \varphi_i, r_i) \approx r_i - R\psi_{k,i}(\theta_i, \varphi_i) + \frac{R^2}{2r_i}\left(1 - \psi_{k,i}^2(\theta_i, \varphi_i)\right) \tag{3}$$

where $R \ll r$, substituting Eq. (3) into Eq. (1) yields

$$x_k(t) = \sum_{i=1}^{N_N} s_i(t) e^{\frac{j2\pi R}{\lambda}\left\{\psi_{k,i}(\theta_i,\varphi_i) - \frac{R}{2r_i}(1-\psi_{k,i}^2(\theta_i,\varphi_i))\right\}} + \sum_{i=1+N_N}^{N_N+N_F} s_i(t) e^{\frac{j2\pi R}{\lambda}\psi_{k,i}(\theta_i,\varphi_i)} + n(t) \tag{4}$$

In matrix form, Eq. (1) can be written as

$$\mathbf{x}(t) = \mathbf{A}_N\mathbf{S}_N(t) + \mathbf{A}_F\mathbf{S}_F(t) + \mathbf{n}(t) \tag{5}$$

where $\mathbf{x}(t)$ and $\mathbf{n}(t)$ are $M \times 1$ dimensional complex vectors.

$$\mathbf{A}_N = [\mathbf{a}_N(\theta_1, \varphi_1, r_1), \mathbf{a}_N(\theta_2, \varphi_2, r_2), \ldots, \mathbf{a}_N(\theta_{N_N}, \varphi_{N_N}, r_{N_N})] \tag{6}$$

$$\mathbf{A}_F = [\mathbf{a}_F(\theta_1, \varphi_1), \mathbf{a}_F(\theta_2, \varphi_2), \ldots, \mathbf{a}_F(\theta_{N_F}, \varphi_{N_F})] \tag{7}$$

$$\mathbf{a}_N(\theta, \varphi, r) = [e^{\frac{j2\pi R}{\lambda}\left\{\psi_1(\theta,\varphi) - \frac{R}{2r}(1-\psi_1^2(\theta,\varphi))\right\}}, \ldots, e^{\frac{j2\pi R}{\lambda}\left\{\psi_M(\theta,\varphi) - \frac{R}{2r}(1-\psi_M^2(\theta,\varphi))\right\}}]^T \tag{8}$$

$$\mathbf{a}_F(\theta, \varphi) = [e^{\frac{j2\pi R}{\lambda}\psi_1(\theta,\varphi)}, \ldots, e^{\frac{j2\pi R}{\lambda}\psi_M(\theta,\varphi)}]^T \tag{9}$$

where $\psi_k(\theta,\varphi) = \cos(\gamma_k - \theta)\sin(\varphi)$, $k = 1, 2, \ldots, M$. Eqs. (8) and (9) represent the steering vector of NFSs and FFSs, respectively. And the superscript T denotes the transpose operator. In addition, the assumptions are required to point out. The source signals are statistically independent processes, which are also independent from the source signals. For the rest of this paper, the following assumptions are need to hold:

1) The source signals are statistically mutually independent, uncorrelated narrowband stationary processes.
2) The sensor noise is spatially uniform white and independent from the signals.

3. THE PROPOSED ALGORITHM

In this section, we will give the algorithm which estimates DOAs of all FFSs and NFSs firstly, then classifies the FFSs and NFSs and estimates the ranges of NFSs lastly.

3.1. DOA Estimation of the Far-Field and Near-Field Sources

For the MUSIC algorithm using high-order cumulant to estimate DOAs of all signals, we should build a new cumulant of the sensor outputs. Assume that M is even, and the four-order cumulant is used to make the cumulant matrix, which can be shown in Eqs. (8)–(11):

$$C_{11} = \mathbf{cum}\left\{x_p(n)\, x^*_{M/2+p}(n)\, x^*_q(n)\, x_{M/2+q}(n)\right\} = \sum_{i=1}^{N_N+N_F} C_{4,i} e^{j\frac{4\pi R}{\lambda}\{\psi_{p,i}(\theta_i,\varphi_i)-\psi_{q,i}(\theta_i,\varphi_i)\}} \quad (10)$$

$$C_{12} = \mathbf{cum}\left\{x_p(n)\, x^*_{p-M/2}(n)\, x^*_q(n)\, x_{M/2+q}(n)\right\} = \sum_{i=1}^{N_N+N_F} C_{4,i} e^{j\frac{4\pi R}{\lambda}\{\psi_{p,i}(\theta_i,\varphi_i)-\psi_{q,i}(\theta_i,\varphi_i)\}} \quad (11)$$

$$C_{13} = \mathbf{cum}\left\{x_p(n)\, x^*_{M/2+p}(n)\, x^*_q(n)\, x_{q-M/2}(n)\right\} = \sum_{i=1}^{N_N+N_F} C_{4,i} e^{j\frac{4\pi R}{\lambda}\{\psi_{p,i}(\theta_i,\varphi_i)-\psi_{q,i}(\theta_i,\varphi_i)\}} \quad (12)$$

$$C_{14} = \mathbf{cum}\left\{x_p(n)\, x^*_{p-M/2}(n)\, x^*_q(n)\, x_{q-M/2}(n)\right\} = \sum_{i=1}^{N_N+N_F} C_{4,i} e^{j\frac{4\pi R}{\lambda}\{\psi_{p,i}(\theta_i,\varphi_i)-\psi_{q,i}(\theta_i,\varphi_i)\}} \quad (13)$$

where $C_{4,i} = \mathbf{cum}\{s_i(t)s_i^*(t)s_i^*(t)s_i^(t)\}$ is the four-order cumulant of the i-th signal; the superscript $*$ represents the complex conjugate; $n = 1, 2, \ldots, N_p$ represents snapshot number.

Here, $p \in [1, M/2]$ and $q \in [1, M/2]$ for Eq. (10), $p \in [1 + M/2, M]$ and $q \in [1, M/2]$ for Eq. (11), $p \in [1, M/2]$ and $q \in [1 + M/2, M]$ for Eq. (12), $p \in [1 + M/2, M]$ and $q \in [1 + M/2, M]$ for Eq. (13).

We can only estimate the DOAs of the signals without r in Eqs. (10)–(13). $\mathbf{C}_{11}$, $\mathbf{C}_{12}$, $\mathbf{C}_{13}$ and $\mathbf{C}_{14}$ that are all the $(M/2) \times (M/2)$ matrices are combined into a matrix. This $M \times M$ matrix $\mathbf{C}_1$ can be constructed as follows:

$$\mathbf{C}_1 = \begin{bmatrix} \mathbf{C}_{11} & \mathbf{C}_{13} \\ \mathbf{C}_{12} & \mathbf{C}_{14} \end{bmatrix} = \begin{bmatrix} \mathbf{G}_1 \\ \mathbf{H}_1 \end{bmatrix} \quad (14)$$

where $\mathbf{G}_1$ is a $\bar{K} \times M$ matrix, and $\mathbf{H}_1$ is a $(M - \bar{K}) \times M$ matrix. We can use the virtual steering matrix to estimate the DOAs, which can be written as

$$\mathbf{A}_{V1} = [\mathbf{a}(\theta_1,\varphi_1), \ldots, \mathbf{a}(\theta_{N_N+N_F}, \varphi_{N_N+N_F})] \quad (15)$$

$$\mathbf{a}(\theta_i,\varphi_i) = \left[e^{\frac{j4\pi R}{\lambda}\psi_{1,i}(\theta_i,\varphi_i)}, \ldots, e^{\frac{j4\pi R}{\lambda}\psi_{M,i}(\theta_i,\varphi_i)}\right]^T \quad (16)$$

$\mathbf{A}_{V1}$ is a $M \times (N_F + N_N)$ matrix. Using Eq. (15), Eq. (14) can be expressed as

$$\mathbf{C}_1 = \mathbf{A}_{V1}\mathbf{C}_s\mathbf{A}_{V1}^H = \begin{bmatrix} \bar{\mathbf{A}}_1 \\ \bar{\mathbf{A}}_2 \end{bmatrix} \mathbf{C}_s \begin{bmatrix} \bar{\mathbf{A}}_1 \\ \bar{\mathbf{A}}_2 \end{bmatrix}^H \quad (17)$$

$\bar{\mathbf{A}}_1$ is a $\bar{K} \times M$ matrix, and $\bar{\mathbf{A}}_2$ is a $(M-\bar{K}) \times M$ matrix. The superscript H is the conjugate transpose operator. Equivalently, $\bar{\mathbf{A}}_2 = \mathbf{P}_{\alpha n}\bar{\mathbf{A}}_1$. Then, $\mathbf{P}_{\alpha n}$ can be obtained.

$$\hat{\mathbf{P}}_{\alpha n} = \left(\mathbf{G}_1\mathbf{G}_1^H\right)^{-1}\mathbf{G}_1\mathbf{H}_1^H \tag{18}$$

We can easily get

$$\mathbf{E}_{\alpha n}\mathbf{A}_{V1} = \mathbf{O} \tag{19}$$

where $\mathbf{E}_{\alpha n} = [\hat{\mathbf{P}}_{\alpha n}^T \ \ -\mathbf{I}^T]^T$, $\mathbf{I} \in C^{M-\bar{K}\times M-\bar{K}}$ is an identity matrix, and $\mathbf{O}$ is a zero matrix. Evidently, the columns of $\mathbf{E}_{\alpha n}$ form a basis of the null space of $\mathbf{A}_{V1}$, so the orthogonal projector is expressed as

$$\mathbf{U}_{\alpha n} = \mathbf{E}_{\alpha n}\left(\mathbf{E}_{\alpha n}^H\mathbf{E}_{\alpha n}\right)^{-1}\mathbf{E}_{\alpha n}^H \tag{20}$$

which is used to obtain $\mathbf{U}_{\alpha n}^H\mathbf{A}_{V1} = \mathbf{O}$. When the finite snapshots of array data are available, the DOAs of all signals can be estimated by the minimizing argument of the cost function:

$$f_1(\theta,\varphi) = \mathbf{a}^H(\theta,\varphi)\mathbf{U}_{\alpha n}\mathbf{U}_{\alpha n}^H\mathbf{a}(\theta,\varphi) \tag{21}$$

where $\mathbf{a}(\theta,\varphi) = [e^{\frac{j4\pi R}{\lambda}\psi_1(\theta,\varphi)},\ldots,e^{\frac{j4\pi R}{\lambda}\psi_M(\theta,\varphi)}]^T$.

3.2. Distinction of the Far-Field and Near-Field Sources

For distinguishing the FFSs and NFSs, we need to build the second cumulant matrix $\mathbf{C}_2$, which is used to estimate the ranges of the NFSs. To utilize signal information adequately, a $M \times M$ matrix is built using the four-order cumulant. Here, $p \in [1, M]$ and $q \in [1, M]$ for Eq. (22).

$$\begin{aligned} C_2 &= \mathbf{cum}\left\{x_p(n)\,x_M^*(n)\,x_q^*(n)\,x_M(n)\right\} \\ &= \sum_{i=1}^{N_N} C_{4,i}e^{\frac{j2\pi R}{\lambda}\left\{\psi_{p,i}(\theta_i,\varphi_i)-\psi_{q,i}(\theta_i,\varphi_i)-\frac{R}{2r_i}(\psi_{p,i}^2(\theta_i,\varphi_i)-\psi_{q,i}^2(\theta_i,\varphi_i))\right\}} \\ &\quad + \sum_{i=1+N_N}^{N_N+N_F} C_{4,i}e^{\frac{j2\pi R}{\lambda}(\psi_{p,i}(\theta_i,\varphi_i)-\psi_{q,i}(\theta_i,\varphi_i))} \end{aligned} \tag{22}$$

Using eigenvalue decomposition, $\mathbf{C}_2$ can be written as

$$\mathbf{C}_2 = \mathbf{\Sigma}_{s2}\mathbf{U}_s\mathbf{\Sigma}_{s2}^H + \mathbf{\Sigma}_{n2}\mathbf{U}_n\mathbf{\Sigma}_{n2}^H \tag{23}$$

where the $(N_F+N_N)\times(N_F+N_N)$ matrix $\mathbf{U}_s$ contains the (N_F+N_N) signal subspace eigenvalues of $\mathbf{C}_2$, and the $M \times (N_F+N_N)$ matrix $\mathbf{\Sigma}_{s2}$ spans the signal subspace of $\mathbf{C}_2$. In turn, the $M \times (M-N_F-N_N)$ matrix $\mathbf{\Sigma}_{n2}$ spans the noise subspace of $\mathbf{C}_2$. Generally, the eigenvalues of the signal subspace are larger than those of the noise subspace.

Before estimating the ranges of the NFSs, we should select the NFSs from all of the signals. Assume that all of the signals are the FFSs. Using the MUSIC algorithm, we put all of DOA estimated by Eq. (21) into Eq. (24). When $f_2(\hat{\theta}_i,\hat{\varphi}_i) \gg 0$, the i-th signal is the FFS. On the contrary, this signal is the NFS.

Here, $\mathbf{bs}^H(\theta,\varphi)$ is the virtual steering matrix that is the same as Eq. (9).

$$f_2\left(\hat{\theta},\hat{\varphi}\right) = \left(\mathbf{bs}^H(\hat{\theta},\hat{\varphi})\mathbf{U}_n\mathbf{U}_n^H\mathbf{bs}(\hat{\theta},\hat{\varphi})\right)^{-1} \tag{24}$$

3.3. Range Estimation of the Near-Field Signals

It is clear that 1D-MUSIC algorithm like Eq. (25) can be used to estimate the $r_i(i = 1, 2, \ldots, N_N)$ since $\hat{\theta}_i$ and $\hat{\varphi}_i$ have been obtained.

$$f_3\left(\hat{\theta}_i,\hat{\varphi}_i,r_i\right) = \left(\mathbf{as}^H\left(\hat{\theta}_i,\hat{\varphi}_i,r_i\right)\mathbf{U}_n\mathbf{U}_n^H\mathbf{as}\left(\hat{\theta}_i,\hat{\varphi}_i,r_i\right)\right)^{-1} \tag{25}$$

where $\mathbf{as}^H(\theta,\varphi,r)$ is the virtual steering matrix that is the same as Eq. (8).

4. COMPUTER SIMULATION RESULTS

In this section, some simulation results are given to evaluate the performance of the proposed algorithm. For the first and second examples, an eight-sensor symmetric UCA with $R = \lambda$ is given. Two equal power narrowband signals (one NFS and one FFS) are impinging on this array. The additive noise is supposed to be spatial white complex Gaussian random process. And the signal-to-noise ratio (SNR) is defined relative to each signal. For the comparison, we execute the TSMUSIC [11] using $R_{k,l} = E\{x_k x_l^*\}(k, l = 1, 2, \ldots, M)$ by eigen value decomposition (EVD), which estimates firstly DOAs of all FFSs and NFSs and then estimates the ranges of NFSs, execute the TSMD [7] that distinguishes firstly the FFSs and NFSs and then estimates the locations of FFSs and NFSs respectively, and execute the related Cramer-Rao Bound (CRB). The results shown next are evaluated by the estimated root man square error (RMSE) from the average results of 200 independent Monte-Carlo simulations.

In the first experiment, we consider the simulation that there are a NFS and a FFS incoming on the sensor array, and their DOAs are similar ((152.1°, 33.2°) and (160.3°, 33.2°, 6.1λ)). The SNR and the snapshot number are set at 20 dB and 1200, respectively. The spatial spectrum of the proposed algorithm and TSMUSIC [11] is shown in Fig. 1. From this figure, the proposed algorithm gives the two peaks for these two signals, which successfully yields DOA estimations for both NFS and FFS. However, the TSMUSIC [11] only gives a peak for these two signals, that is, which cannot give the right DOA for the NFS so that it is invalid for the similar DOAs of two signals. So, our algorithm can achieve a more reasonable classification for the signals than TSMUSIC [11].

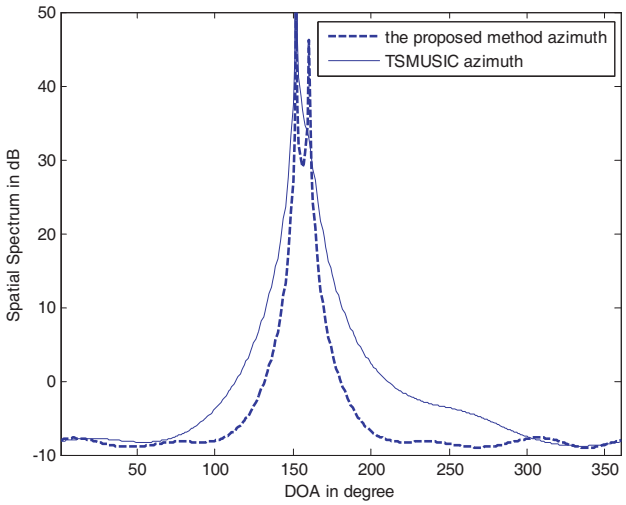

Figure 1. Spatial spectrum of azimuth estimation. (152.1°, 33.2°) and (160.3°, 33.2°, 6.1λ), SNR = 10 dB, the snapshot number is 2000.

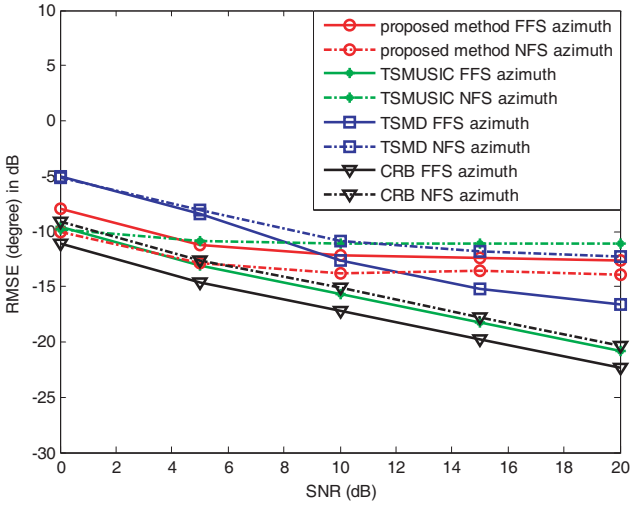

Figure 2. RMSEs of azimuth angles estimations for mixed NFSs and FFSs versus SNRs. (82.5°, 33.2°) and (160.3°, 62.1°, 6.1λ), the snapshot number is 2000. 200 independent trails.

In the second experiment, the performance of the proposed algorithm in the scenario where an FFS and a NFS exist simultaneously is assessed, which are located at (82.5°, 33.2°) and (160.3°, 62.1°, 6.1λ), respectively. We determine the SNR from 0 to 20 dB, and 200 independent trails and the other simulation conditions are similar to the first experiment. The RMSEs of the azimuth angles, elevation angles and the range estimations by the proposed algorithm are presented in Fig. 2, Fig. 3 and Fig. 4, respectively. Meanwhile, the TSMUSIC [11] algorithm, the TSMD [7] algorithm and the related CRB are also represented for comparison. What we can see from these figures are that the proposed algorithm has lower accuracy than TSMUSIC [11] and TSMD [7] at high SNR for the DOA of FFS, but it has higher accuracy than TSMD [7] at low SNR. At the same time, there is higher accuracy for the DOA of NFS in the proposed algorithm than that in TSMUSIC [11] and in TSMD [7] from Fig. 2 and Fig. 3. For the range of NFS estimation, the proposed algorithm has almost the same accuracy as TSMUSIC [11] and TSMD [7].

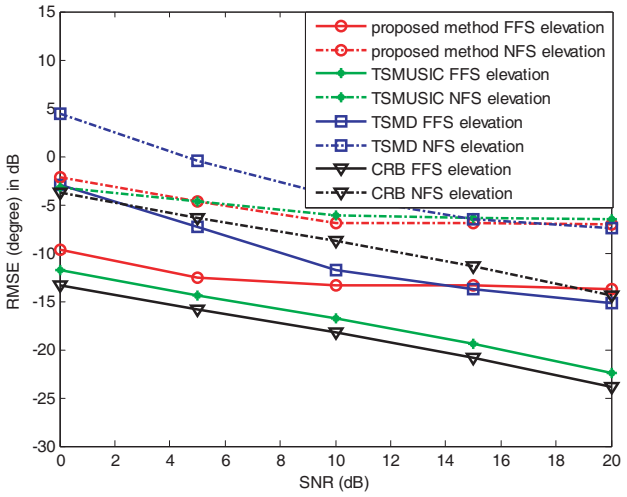

Figure 3. RMSEs of elevation angles estimations for mixed NFSs and FFSs versus SNRs. (82.5°, 33.2°) and (160.3°, 62.1°, 6.1λ), the snapshot number is 2000. 200 independent trails.

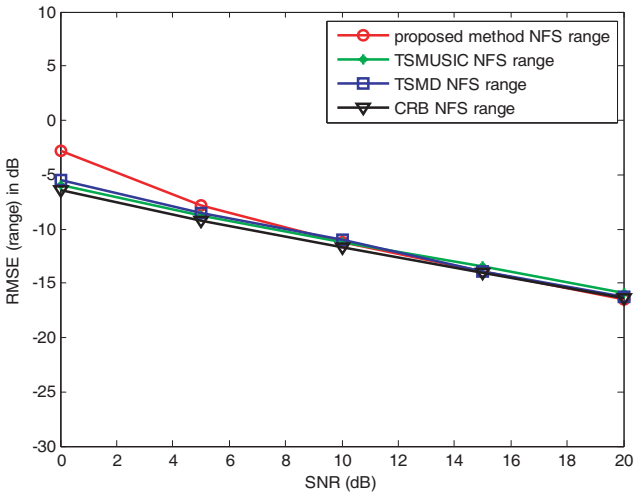

Figure 4. RMSEs of range estimations for mixed NFSs and FFSs versus SNRs. (82.5°, 33.2°) and (160.3°, 62.1°, 6.1λ), the snapshot number is 2000. 200 independent trails.

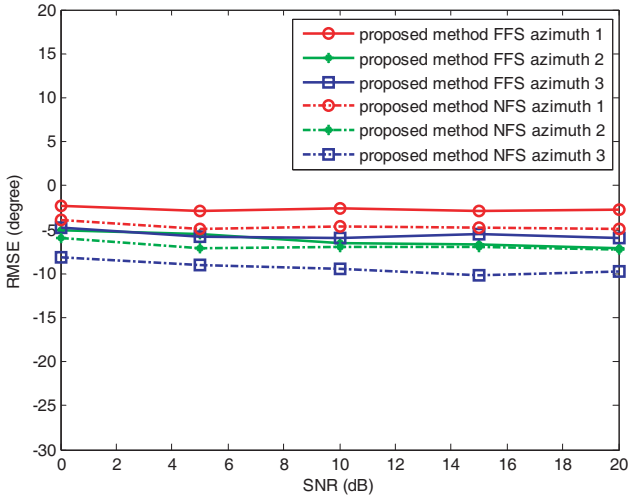

Figure 5. RMSEs of azimuth angles estimations for mixed NFSs and FFSs versus SNRs. (22.10°, 33.20°), (61.74°, 41.06°, 2.5λ), (101.38°, 48.92°, 3.2λ), (141.02°, 56.78°, 4.1λ), (180.66°, 64.64°) and (220.03°, 72.50°). The snapshot number is 2000. 200 independent trails.

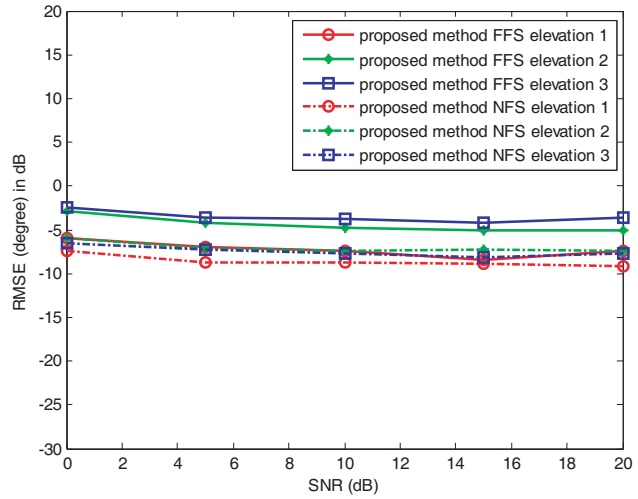

Figure 6. RMSEs of elevation angles estimations for mixed NFSs and FFSs versus SNRs. (22.10°, 33.20°), (61.74°, 41.06°, 2.5λ), (101.38°, 48.92°, 3.2λ), (141.02°, 56.78°, 4.1λ), (180.66°, 64.64°) and (220.03°, 72.50°). The snapshot number is 2000. 200 independent trails.

In the third experiment, a sixteen-sensor symmetric UCA with $R = \lambda$ is given. Six equal power narrowband signals (three NFSs and three FFSs) are impinging on this array. These signals are located at (22.10°, 33.20°), (61.74°, 41.06°, 2.5λ), (101.38°, 48.92°, 3.2λ), (141.02°, 56.78°, 4.1λ), (180.66°, 64.64°) and (220.03°, 72.50°), respectively. The other simulation conditions are similar to the first experiment. The RMSEs of the azimuth angles, elevation angles and the range estimations by the proposed algorithm are presented in Fig. 5, Fig. 6 and Fig. 7, respectively. From these figures, the proposed algorithm represents a better estimation in NFSs. Compared with the case where one NFS and one FFS are impinging on the array, it has lower accuracy in this case. Yet, its performance is still great in mixed multi-source localization.

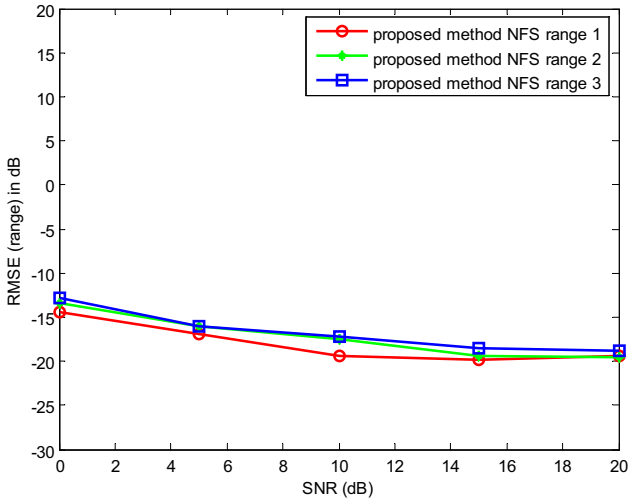

Figure 7. RMSEs of range estimations for mixed NFSs and FFSs versus SNRs. (22.10°, 33.20°), (61.74°, 41.06°, 2.5λ), (101.38°, 48.92°, 3.2λ), (141.02°, 56.78°, 4.1λ), (180.66°, 64.64°) and (220.03°, 72.50°). The snapshot number is 2000. 200 independent trails.

5. COMPUTATIONAL COMPLEXITY

For the computational complexity, we consider the major multiplications existing in matrix construction, EVD computation, and MUSIC spectrum search. The TSMUSIC method [11] contains one $M \times M$ matrix, performs its EVD, and needs one two-dimensional DOA search and N_N times range search. Hence, the multiplications are estimated by

$$O\left(M^2 N_p + \frac{4}{3}M^3 + \frac{360}{\delta_\theta}\frac{180}{\delta_\varphi}M^2 + N_N\frac{Len}{\delta_r}M^2\right) \tag{26}$$

where N_p represents the snapshot number; δ_θ and δ_φ denote the search step of DOA; δ_r is the search step of range; Len is the length of range search. The TSMD method [7] contains one $M \times M$ matrices, builds one difference matrix, executes the EVD of two matrices, as well as performs twice two-dimensional DOA search and N_N times range search. Hence, the multiplications are estimated by

$$O\left(M^2 N_p + 2M^2 + \frac{8}{3}M^3 + 2\frac{360}{\delta_\theta}\frac{180}{\delta_\varphi}M^2 + N_N\frac{Len}{\delta_r}M^2\right) \tag{27}$$

Similarly, the proposed method contains two $M \times M$ matrices, executes the EVD of one matrix, as well as performs twice two-dimensional DOA search and N_N times range search. Hence, the multiplications are estimated by

$$O\left(3M^2 N_p + \frac{4}{3}M^3 + 2\frac{360}{\delta_\theta}\frac{180}{\delta_\varphi}M^2 + N_N\frac{Len}{\delta_r}M^2\right) \tag{28}$$

We can find that the TSMUSIC method [11] has the lowest computational complexity, and the proposed method has higher computational complexity than the TSMUSIC method [11] and TSMD method [7].

6. CONCLUSIONS

This paper gives a three-dimensional scenario for mixed NFSs and FFSs localization using UCA and presents an efficient three-stage MUSIC algorithm for this scenario. Our investigation shows that the novel algorithm has higher resolution than TSMUSIC [11]. Compared to the TSMUSIC [11] and TSMD [7], the proposed solution is more efficient and has higher accuracy for the DOA estimations of the NFS. In addition, the proposed method has disadvantage in computational complexity.

REFERENCES

1. Krim, H. and M. Viberg, "Two decades of array signal processing research: The parametric approach," *IEEE Signal Processing Magazine*, Vol. 13, No. 4, 67–94, 1996.
2. Schmidt, R. O., "Multiple emitter location and signal parameter estimation," *IEEE Transactions on Antennas and Propagation*, Vol. 34, No. 3, 276–280, 1986.
3. Rot, R. and T. Kailath, "Esprit-estimation of signal parameters via rotational invariance techniques," *IEEE Transactions on Acoustics, Speech, and Signal Processing*, Vol. 37, No. 7, 984–995, 1989.
4. Liang, J. and D. Liu, "Passive localization of mixed near-field and far-field sources using two-stage music algorithm," *IEEE Transactions on Signal Processing*, Vol. 58, No. 1, 108–120, 2010.
5. Wang, B., Y. Zhao, and J. Liu, "Mixed-order MUSIC algorithm for localization of far-field and near-field sources," *IEEE Signal Processing Letters*, Vol. 20, No. 4, 2013.
6. Jiang, J., F. Duan, J. Chen, Y. Li, and X. Hua, "Mixed near-field and far-field sources localization using the uniform linear sensor array," *IEEE Sensors Journal*, Vol. 13, No. 8, 3136–3143, 2013.
7. Liu, G. and X. Sun, "Two-stage matrix differencing algorithm for mixed far-field and near-field sources classification and localization," *IEEE Sensors Journal*, Vol. 14, No. 6, 1957–1965, 2014.
8. Xie, J., H. Tao, X. Rao, and J. Su, "Passive localization of mixed far-field and near-field sources without estimating the number of sources," *Sensors*, Vol. 15, No. 15, 3834–3853, 2015.
9. Tao, H., J. Xin, J. Wang, N. Zheng, and A. Sano, "Two-dimensional direction estimation for a mixture of noncoherent and coherent signals," *IEEE Transactions on Signal Processing*, Vol. 63, No. 2, 318–333, 2015.
10. Wang, G., J. Xin, N. Zheng, and A. Sano, "Computationally efficient subspace-based algorithm for two-dimensional direction estimation with L-shaped array," *IEEE Transactions on Signal Processing*, Vol. 59, No. 7, 3197–3212, 2011.
11. Wu, Y., H. Wang, Y. Zhang, and Y. Wang, "Multiple near-field source localisation with uniform circular array," *Electronics Letters*, Vol. 49, No. 24, 1509–1510, 2013.
12. Jung, T. and K. Lee, "Closed-form algorithm for 3-D single-source localization with uniform circular array," *IEEE Antennas Wireless Propagation Letters*, Vol. 13, No. 6, 1096–1099, 2014.
13. Liao, B., Y. Wu, and S. Chan, "A generalized algorithm for fast two dimensional angle estimation of a single source with uniform circular array," *IEEE Antennas Wireless Propagation Letters*, Vol. 11, 984–986, 2012.